Nuclear Instruments and Methods in Physics Research A275 (1989) 246–257
North-Holland, Amsterdam

# PERFORMANCE OF A Pb–Cu LIQUID ARGON CALORIMETER WITH AN IRON STREAMER TUBE TAIL CATCHER

W. BRAUNSCHWEIG, F.J. KIRSCHFINK, J. TUTAS and E. VOGEL
*I Physikalisches Institut der RWTH Aachen, FRG* *

M. WIDGOFF
*Department of Physics, Brown University, Providence, USA*

F.W. BRASSE, W. FLAUGER, J. GAYLER, V. KORBEL, J. MARKS and C. ZEITNITZ
*Deutsches Elektronen Synchrotron, DESY, Hamburg, FRG*

F. BRINKER, S. BRINKMANN, P. HARTZ, K. RAUSCHNABEL, A. WALTHER and D. WEGENER
*Institut für Physik, Universität Dortmund, FRG* **

V. BRISSON, D. LELLOUCH [+], P. PERRODO and C. VALLÉE
*Ecole Polytechnique, Palaiseau, France*

A.J. CAMPBELL
*University of Glasgow, UK*

K. LAU, F. LIPP and R. WEINSTEIN
*Department of Physics, University of Houston, USA*

H.T. BLUME, H. GREIF, J. HUBER, C. KIESLING [++], D. LÜERS, H. OBERLACK and P. SCHACHT
*Max-Planck-Institut für Physik und Astrophysik, München, FRG*

E. VON GOELER and J. MOROMISATO
*Department of Physics, Northeastern University, Boston, USA*

B. DELCOURT and A. JACHOLKOWSKA
*Laboratoire de l'Accélérateur Linéaire, Orsay, France*

E. BARRELET, J. DUBOC and H.K. NGUYEN
*Laboratoire de la Physique Nucléaire et Hautes Energies, Université de Paris, France*

V. BIDOLI, F. FERRAROTTO and B. STELLA
*INFN e Università di Roma "La Sapienza", Italy*

* Supported by the German Bundesministerium für Forschung und Technologie under contract number 054AC17P.
** Supported by the German Bundesministerium für Forschung und Technologie under contract number 054DO057I.
[+] Now at Weizmann Institute of Science, Israel.
[++] Heisenberg-Stipendiat der Deutschen Forschungsgemeinschaft.

0168-9002/89/$03.50 © Elsevier Science Publishers B.V.
(North-Holland Physics Publishing Division)

M. BESANÇON, G. COZZIKA, M. DAVID, J. FELTESSE, A. DE LESQUEN, P. VERRECCHIA and G. VILLET

*Centre d'Étude Nucléaires, Saclay, France*

U. STRAUMANN

*Physikalisches Institut der Universität Zürich, Switzerland*

Received 21 September 1988

A lead–copper calorimeter in liquid argon and an iron streamer tube calorimeter acting as a tail catcher have been tested with pions in the energy range of 30–230 GeV. Results are given on the energy resolution, on sampling fluctuations and on the space resolution of the liquid argon calorimeter. For the combined system an energy resolution of $\sigma/E \approx 0.5/\sqrt{E}$ is obtained applying software weighting techniques and corrections for the dead material between the two calorimeters on an event to event basis. The remaining tails in the energy distributions are discussed.

## 1. Introduction

We have reported recently on calorimeter tests in preparation of the forthcoming H1 experiment at HERA using electron and pion beams at CERN. We presented results for a liquid argon (LAr) calorimeter [1] with lead and copper absorber plates and also for a streamer tube calorimeter [2] with iron absorbers. It was verified [1] that the energy resolution of the LAr calorimeter can be considerably improved by corrections of $\pi^0$ fluctuations and achieved an energy resolution for incident pions of $\sigma/E \approx 0.50/\sqrt{E}$ selecting events with no energy leakage out of the LAr calorimeter. The performance of the iron streamer tube calorimeter in a stand alone mode was discussed in ref. [2] and an energy resolution of $\sigma/E \approx 1.0/\sqrt{E}$ was obtained for fully contained pion initiated showers.

Here we report on the system of the LAr calorimeter combined with the streamer tube calorimeter which acts as a tail catcher. In section 2 we give a short description of the experimental setup. The calibration procedures for both calorimeters are outlined in section 3. The performance of the combined system is discussed in section 4, where we also present new results of the LAr calorimeter alone.

The setup described here corresponds to the planned H1 experiment under an angle of about 45° with respect to the depths of the calorimeters involved. The calorimeters were steps towards the H1 calorimeter; they are, however, no real prototypes.

## 2. Experimental setup

The test beam, the beam detectors, trigger system, the LAr calorimeter and the iron streamer tube calorimeter have been described in detail in refs. [1,2]. Only a short repetition is given here and some minor changes of the tail catcher calorimeter with respect to ref. [2] are outlined. The whole setup is shown in fig. 1.

### 2.1. The LAr calorimeter

The LAr calorimeter ("setup B" in ref. [1]) is divided into two parts, a front section used as electromagnetic calorimeter (EC) with a depth of 26 radiation length ($X_0$) (1.1 interaction length ($\lambda$)) and a hadronic calorimeter (HC) with a depth of 6.1$\lambda$.

The EC consists of lead plates of 2.4 mm thickness with a special high voltage system using high resistive foils glued either on the lead plates or on the readout boards (ROBs). The LAr gap is on average 2.8 mm wide. The 48 pads of the ROBs with a size of $3.0 \times 3.0$ cm$^2$ in the central region and $6.0 \times 7.5$ cm$^2$ respectively $7.5 \times 7.5$ cm$^2$ in the outer region are longitudinally ganged together leading to a 5-fold longitudinal segmentation.

The HC has copper absorber plates with a thickness of 5.0 mm. The ROBs are centered between two copper plates forming two LAr gaps of 1.5 mm thickness on each side. A strip pattern ($8.0 \times 40.0$ cm$^2$) orientated in

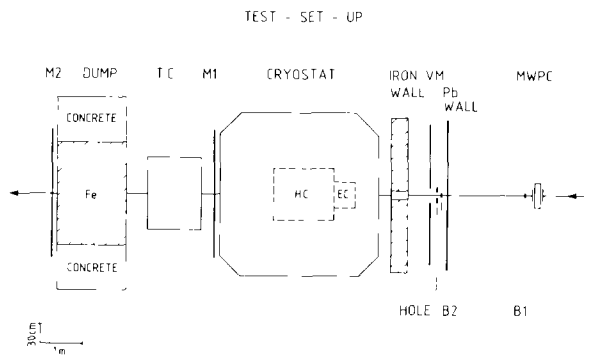


Fig 1 Layout of the experimental area.

Table 1
Technical parameters of the LAr calorimeter

| | EC | HC |
|---|---|---|
| Absorber material | lead | copper |
| Size of the plates ($mm^3$) | $2.4\times420\times420$ | $5.0\times820\times800$ |
| LAr gap (mm) | 2.8 | $2\times1.5$ |
| ROB position | on lead plate | central in gap |
| Length (mm/λ) | 377.5/1.13 | 1391/6.12 |
| Longitudinal segmentation | 2.7/3.6/3.6/3.6/ 12.6 $X_0$ | $6\times1.02\lambda$ |
| Pad size ($cm^2$) | $3\times3/6\times7.5/$ $7.5\times7.5$ | $40\times8$ |
| Number of ROBs | 57 | 154 |
| Number of electronic channels | 240 | 240 |

horizontal ($y$-strips) and vertical ($x$-strips) direction alternating from board to board performs an interleaved tower structure by ganging together the corresponding strips of the same orientation. This leads to a 6-fold longitudinal segmentation of a length of 1.0λ each.

The parameters of the LAr calorimeter are summarized in table 1.

### 2.2. The tail catcher calorimeter

The tail catcher calorimeter (TC) consists of iron plates interleaved with streamer tube planes (single cell size $9\times9$ $mm^2$) as active elements. The sampling thickness amounts to 7.5 cm, and the total thickness of 75 cm corresponds to 4.5λ. The active area is about 1 $m^2$. The arrangement of chambers is given in table 2. With respect to ref. [2], three chamber planes with digital readout were added, such that the configuration corresponds to the planned H1 detector [9]. The tubes were operated with the standard gas mixture (25% argon, 75% isobuthane) at 4.7 kV. In order to reduce a negative crosstalk of about 9% on adjacent pads (see ref. [2]), an external HV blocking capacitor of 2.2 nF was added for each HV-line. To avoid the subsequently occurring reflections a series resistor of 1 kΩ was inserted. As a result, the crosstalk was reduced by a factor of two. The electronic threshold for the digital readout was set to a nominal value of 50 mV (see ref. [2]), leading to an average multiplicity of 1.6 streamers per minimum ionizing particle per plane and an efficiency of 90%.

Table 2
Location of the different layers in the tail catcher calorimeter.

| Layer no. | Iron depth (cm) | Equipped with | | | Tower no. |
|---|---|---|---|---|---|
| | | Pads | Parallel strips | Orthogonal strips | |
| 1 | 0.0 | | * | * | |
| 2 | 0.0 | | * | * | |
| 3 | 0.0 | * | | | [a] |
| 4 | 7.5 | * | * | | 1 |
| 5 | 15.0 | * | * | | 1 |
| 6 | 22.5 | * | * | | 1 |
| 7 | 30.0 | * | * | | 1 |
| 8 | 30.0 | | * | * | |
| 9 | 37.5 | * | * | | 1 |
| 10 | 45.0 | * | * | | 2 |
| 11 | 52.5 | * | * | | 2 |
| 12 | 60.0 | * | * | | 2 |
| 13 | 67.5 | * | * | | 2 |
| 14 | 75.0 | * | | | 2 |
| 15 | 75.0 | | * | * | |
| 16 | 75.0 | | * | * | |

[a] Presampler.

Table 3
Inactive material between the LAr calorimeter and the tail catcher calorimeter.

| Material | Thickness (cm) |
|---|---|
| Last Cu plate | 0.5 |
| Steel plate | 2.5 |
| Al plate | 2.5 |
| LAr | 88.3 |
| Cryostat wall (steel) | 0.5 |
| Foam | 40.0 |
| Cryostat wall (Al) | 0.1 |
| Air | 15.0 |
| Scintillator wall | 1.0 |
| Total (cm/λ) | 148/1.4 |

The calorimeter was mounted behind the cryostat of the LAr calorimeter (fig. 1). The materials between the two calorimeter which amount to 1.4λ are listed in table 3.

## 3. Data analysis

### 3.1. Calibration of the LAr calorimeter

The calibration of the LAr calorimeter consists of two parts:
- the electronic charge calibration,
- the energy calibration using the test beam.

#### 3.1.1. Electronic calibration

The electronic chain is calibrated by feeding a voltage pulse via a $10\pm0.1$ pF capacitor into each preamplifier as described in more detail in ref. [1]. This provides the channel to charge conversion of the ADCs.

#### 3.1.2. Data corrections

The data selection criteria and most of the data corrections have been presented in ref. [1]. Here only

two additional corrections are discussed. For further details see ref. [3].

During the analysis it turned out that the interleaved $x$- and $y$-strips of each section in the HC gave somewhat different response to pions. Therefore the response of the sum over all $x$-strips of a given section were scaled to agree on average with the response of the corresponding sum of $y$-strips. This leads to a correction of less than 4%, apart from the fifth section of the HC where it amounted to 15%.

Considering the correlation between the charge in the third section and the total charge it has been observed that the response of the third section is too high. Fitting a factor between the sum of the charge of the third section and the total charge using fully contained events in the HC with a beam energy of 230 GeV leads to a reduction in amplitude of 16% in the third section. The factor is independent from the beam energy and of the position of the shower vertex.

Both these corrections take care of some possible nonuniformities in the thickness of the LAr gaps, the high voltage supply and the electronic calibration. Due to these corrections the energy resolution is improved by about 10%.

*3.1.3. Energy calibration*

The LAr calorimeter was calibrated allowing only for very little energy leakage out of the calorimeter. Thereby events were rejected where one or more strips fired in the TC. This implies that the showers are nearly fully contained within 8.6λ of which the first 7.2λ are utilized to measure the shower energy. The fraction of events removed by this cut at each beam energy is given in table 4.

*3.1.3.1. Determination of calibration parameters.* To take account of the different sampling ratio and absorber material the total energy for incident pions was calculated by

$$E = c_{\mathrm{EC}} \sum_{\mathrm{EC}} Q_i + c_{\mathrm{HC}} \sum_{\mathrm{HC}} Q_i , \tag{1}$$

where $Q_i$ are the measured charges of the individual channels. The overall calibration factors $c_{\mathrm{EC}}$ and $c_{\mathrm{HC}}$ were determined by minimizing $\sigma/E$ with the constraint of $\langle E \rangle = E_{\mathrm{beam}}$. As is to be expected for a noncompensating calorimeter, the calibration factors decrease by about 7% from 30 to 230 GeV as shown in table 5.

Table 4
Fraction of events vetoed by the tail catcher calorimeter.

| $E$ (GeV) | 30 | 50 | 170 | 230 |
|---|---|---|---|---|
| Fraction | 0.11 | 0.20 | 0.51 | 0.52 |

Table 5
Calibration factors (without $\pi^0$-weighting).

| $E$ (GeV) | 30 | 50 | 170 | 230 |
|---|---|---|---|---|
| $c_{\mathrm{EC}}$ | 3.27 | 3.16 | 3.06 | 3.03 |
| $c_{\mathrm{HC}}$ | 4.60 | 4.53 | 4.34 | 4.42 |

Due to the fact that $e/\pi$ is not equal to 1, the $\pi^0$ fluctuations are deteriorating the energy resolution for hadronic showers as discussed in ref. [1]. The method described here to correct the $\pi^0$ fluctuations on an event to event basis is similar to the approach described in ref. [1]. The measured total energy is calculated by

$$E = c^{\mathrm{w}}_{\mathrm{EC}} \sum_{\mathrm{EC}} Q_i (1 - \eta_{\mathrm{EC}} Q_i) + c^{\mathrm{w}}_{\mathrm{HC}} \sum_{\mathrm{HC}} Q_i (1 - \eta_{\mathrm{HC}} Q_i) \tag{2}$$

with $(1 - \eta_{\mathrm{EC}} Q_i) > \delta$ and $(1 - \eta_{\mathrm{HC}} Q_i) > \delta$, where $Q_i$ are the measured charges of the individual channels, $c^{\mathrm{w}}_{\mathrm{EC}}$ and $c^{\mathrm{w}}_{\mathrm{HC}}$ give the overall calibration of both calorimeter parts, and the factors $(1 - \eta_{\mathrm{EC}} Q_i)$ and $(1 - \eta_{\mathrm{HC}} Q_i)$ suppress large local energy deposits which are presumably due to $\pi^0$ excesses. The numeric values given below for $\eta_{\mathrm{EC}}$ refer to the small pad sizes in the EC; correction factors for larger pads inversely proportional to the pad area have been applied. To simplify the procedure the $\eta_{\mathrm{EC}}$ and $\eta_{\mathrm{HC}}$ operate directly on the measured charges and not on the calibrated tower energies as in ref. [1]. The corrections are limited by the parameter $\delta$.

To arrive at a parametrization of the energy dependence of the five calibration parameters in eq. (2) we proceed as follows. The parameters $\eta_{\mathrm{EC}}$ and $\eta_{\mathrm{HC}}$ were determined separately for each beam energy by minimizing $\sigma/E$ for fixed values of $\delta$. For $\delta$ a linear function of the beam energy has been chosen with the following values: slope $= 4.167 \times 10^{-4}$ GeV$^{-1}$ and constant term $= 0.644$. The best results have been obtained if $\delta$ is taken to be the same for the EC and the HC. With this choice of $\delta$ the weighting parameters $\eta_{\mathrm{EC}}$ and $\eta_{\mathrm{HC}}$ are decreasing slower than $E^{-1}$ as shown in fig. 2. The energy dependence can be parametrized by

$$\eta = \xi / \sqrt{E} \tag{3}$$

(as in ref. [5]). A fit (curve in fig. 2) leads to

$$\xi_{\mathrm{EC}} = 0.93 \quad \sqrt{\mathrm{GeV}}/\mathrm{pC},$$

$$\xi_{\mathrm{HC}} = 1.27 \quad \sqrt{\mathrm{GeV}}/\mathrm{pC}.$$

Using the values $\eta_{\mathrm{EC}}$ and $\eta_{\mathrm{HC}}$ from this parametrization for each beam energy the overall calibration factors $c^{\mathrm{w}}_{\mathrm{EC}}$ and $c^{\mathrm{w}}_{\mathrm{HC}}$ are determined by minimizing $\sigma/E$ with the constraint of $\langle E \rangle = E_{\mathrm{beam}}$. In fig. 3 the calibration factors $c^{\mathrm{w}}_{\mathrm{EC}}$ and $c^{\mathrm{w}}_{\mathrm{HC}}$ are plotted as a function of the beam energy. They are roughly constant over the whole energy range, $c^{\mathrm{w}}_{\mathrm{EC}}$ falling by 3.2%, $c^{\mathrm{w}}_{\mathrm{HC}}$ increasing by

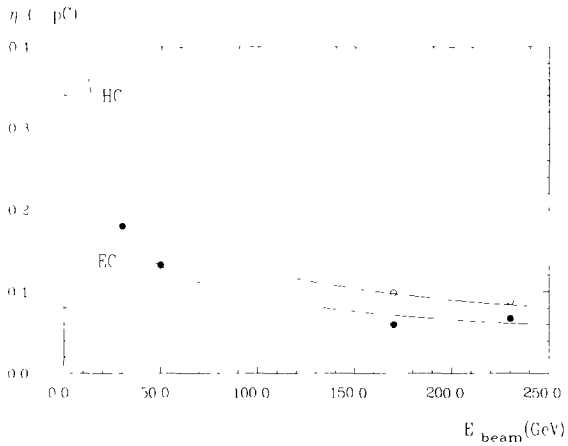


Fig 2 Weighting parameters of EC ($\eta_{EC}$) and HC ($\eta_{HC}$) as function of the beam energy. The full curves are fits according to eq. (3).

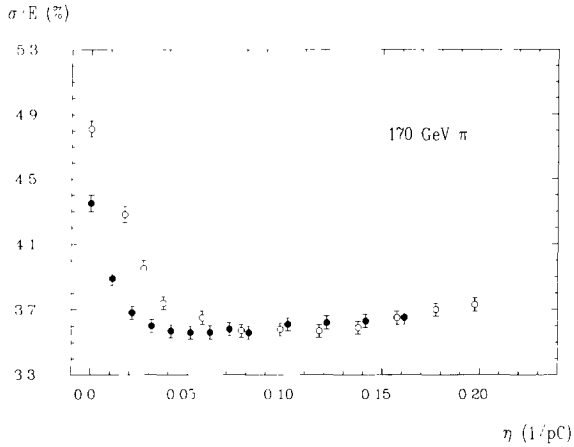


Fig. 4 Energy resolution as a function of the weighting parameter $\eta_{EC}$ (full circles) or $\eta_{HC}$ (open circles) for incident pions of 170 GeV. One of the weighting parameters is fixed to the value given by the parametrization (eq. (3), $\eta_{HC} = 0.097\ pC^{-1}$ and $\eta_{EC} = 0.071\ pC^{-1}$, respectively).

1.2%. The deviations from a linear energy dependence are less than 0.9% for both calibration factors.

With the energy dependence of the parameters $\eta_{EC}$ and $\eta_{HC}$ as given above a good energy resolution is obtained (section 4.1.1), however the parameters can be varied in a wide range without significant loss in energy resolution if the parameters $c^w_{EC}$ and $c^w_{HC}$ are refitted correspondingly. This is demonstrated in fig. 4 for the example of incident pions of 170 GeV.

*3.1.3.2. Energy reconstruction.* The unknown energy of an incident particle is reconstructed using the energy dependence of the calibration parameters as determined above. For each event the first step of the conversion from charge to energy is performed (as in ref. [1]) by using the calibration parameters determined without weighting for $E_{beam} = 50$ GeV. With this first energy value the two sets of ($c^w$, $\eta$, $\delta$) are calculated using the parametrized functions for the EC and HC. These sets of constants are used to obtain with eq. (2) a new value of the energy. This energy value is used to calculate again two new sets of ($c^w$, $\eta$, $\delta$). The final result of the "weighted" energy is obtained after two further steps.

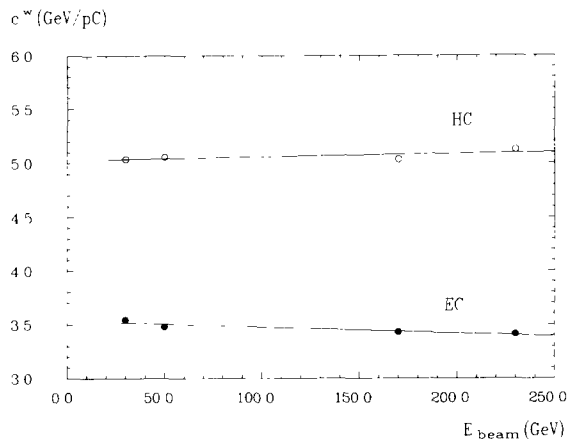


Fig. 3 Overall calibration constants of EC ($c^w_{EC}$, full circles) and HC ($c^w_{HC}$, open circles) as function of beam energy Straight lines: fits used for the energy reconstruction (section 3.1.3).

With this procedure the reconstructed mean energy deviates from the nominal beam energy by less than 0.7% in all four cases. This is still true for special events with the first interaction in the first section of the EC and also for events with less than 5% of the beam energy deposited in the EC. The $e/\pi$ response ratio obtained by comparing incident electrons with incident pions differs by less than 2.5% from 1. As a further test of the quality of the energy reconstruction procedure overlays of different events with $E_{beam} = 30$ GeV have been performed by software. Overlaying $N$ events of $E_{beam} = 30$ GeV ($N = 2, 3, \ldots, 8$) the maximal deviations from $N \times 30$ GeV was below $\pm 0.9\%$.

### 3.2 Calibration of the tail catcher calorimeter

The TC was calibrated with minimum ionizing particles. Muons were selected by using the scintillator hodoscope VM, M1 and M2 (see fig. 1) and a track finding algorithm very similar to the one described in ref. [2]. For the intercalibration, i.e. to ensure an equal response of all towers, we followed exactly the procedure given in ref. [2]. The constant for the absolute calibration was calculated for each run by using the $\mu/\pi$ ratio as measured in ref. [2]: The charge deposited by a muon was equivalent to 2.08 GeV. Due to the

different crosstalk an additional correction of 5% had to be applied. The systematic uncertainty of this absolute calibration was estimated to ±3% which is common to the various runs with the exception of the 230 GeV data. There the muon trigger was not available, therefore the mean muon signal of all other runs was used. In that case, the systematic uncertainty is of the order of 10%.

The total energy deposited in the TC is given by the sum of all analogue channels above threshold. As in ref. [2], this software threshold was set to $2\sigma_{\mathrm{rms}}$ of the noise distribution and corresponded to the charge of half a streamer per tower.

## 4. Performance and results

Results are presented for pion energies of 30, 50, 170 and 230 GeV. In the first part of this section events are treated where the energy is fully contained in the LAr calorimeter. In the second part the combination of the LAr calorimeter with the gas tail catcher is discussed.

### 4.1. LAr calorimeter without tail catcher

Events fully contained in the LAr calorimeter are selected as described in section 3.1.3.

#### 4.1.1. Energy resolution

The reconstruction of the a priori unknown incident particle energy is discussed in section 3.1.3. From Gaussian fits to the obtained energy distributions for each of the four beam energies the resolution is evaluated and is shown in fig. 5. The full curve corresponds to a parametrization of the energy resolution by the expression

$$\frac{\sigma}{E} = \sqrt{\frac{A^2}{E} + \frac{B^2}{E^2} + C^2}, \qquad A^2 = I^2 + S^2, \tag{4}$$

where $I$ represents the intrinsic shower fluctuations, $S$ the sampling fluctuations, $B$ the electronic noise and $C$ a constant term describing beam resolution and intercalibration errors. The contribution of electronic noise to the resolution was determined for each beam energy by random trigger events (see ref. [1]). A fit to the data points in fig. 5 subtracting the electronic noise of about 1.2 GeV yields

$$A = 0.448 \pm 0.005\ \sqrt{\mathrm{GeV}}, \qquad C = 0.016 \pm 0.001.$$

Somewhat more narrow energy distributions are obtained, if the incident particle energy is not reconstructed, but the calibration constants are fixed instead at each energy point to the values given by the parametrization. A fit leads to the values $A = 0.421 \pm 0.005\ \sqrt{\mathrm{GeV}}$ and $C = 0.016 \pm 0.001$.

The widths of the measured energy distributions without corrections for $\pi^0$ fluctuations are also shown in fig. 5. These data points yield the fitted parameters $A = 0.614 \pm 0.006\ \sqrt{\mathrm{GeV}}$ and $C = 0.035 \pm 0.001$.

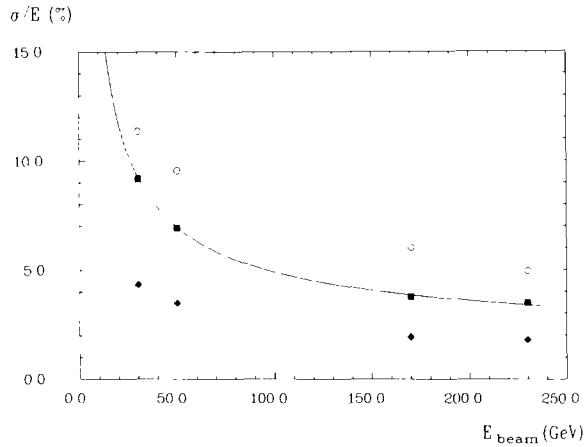


Fig. 5. Energy resolution and sampling term for fully contained events in the LAr calorimeter, open circles: no $\pi^0$ energy weighting; full circles: $\pi^0$ energy weighting; and rhombs: sampling fluctuations. The curve corresponds to the parametrization given by eq. (4) with $A = 0.448\ \sqrt{\mathrm{GeV}}$, $B = 1.2$ GeV and $C = 0.016$

#### 4.1.2. Sampling fluctuations

Two methods are used to determine the sampling fluctuations. As described in section 2.1 the HC has a separated readout of interleaved $x$- and $y$-strips in a given longitudinal segment. Selecting showers nearly fully contained in the HC – by the condition $E_{\mathrm{EC}} < 0.05 E_{\mathrm{beam}}$ – the sampling fluctuations can be extracted using eq. (4)

- from the distribution of the energy difference of the summed $x$- and $y$-strips,
- by comparing the energy distribution of the sum of $x$- and $y$-strips with the single ones.

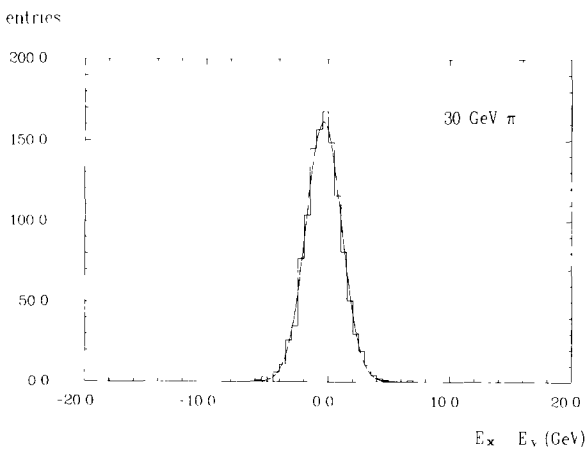


Fig. 6. Distribution of the energy difference of the $x$- and $y$-strips at $E_{\mathrm{beam}} = 30$ GeV.

Table 6
Sampling term.

| | $S$ ($\sqrt{\text{GeV}}$) | $C$ |
|---|---|---|
| Method I without $\pi^0$-weighting | $0.244 \pm 0.004$ | $0.008 \pm 0.001$ |
| Method I with $\pi^0$-weighting | $0.235 \pm 0.004$ | $0.009 \pm 0.001$ |
| Method II | $0.272 \pm 0.029$ | |

Considering the distribution of the energy difference of the $x$- and $y$-strips from eq. (4) we expect
- no contribution from the intrinsic fluctuations,
- no contribution from the correlated electronic noise,
- a reduced constant term.

Fig. 6 shows the distribution of the energy difference of the $x$- and $y$-strips at a beam energy of 30 GeV. The widths of the distributions are obtained by a Gaussian fit for each beam energy. After subtraction of uncorrelated contribution of the electronic noise the dependence

$$\frac{\sigma}{E} = \sqrt{S^2/E + C^2}$$

is used instead of eq. (4) to fit the sampling fluctuations $S$ and the constant term $C$ by a fit to the data. The results are shown in table 6. As to be expected the sampling term stays about the same with the technique of $\pi^0$ energy weighting as without.

The second method comparing the distribution of the sum of the $x$- and $y$-strips with the distribution of the $x$-strips ($y$-strips) has already been discussed in ref. [1], but there without a selection of fully contained events in the HC. The parameters $A$ and $C$ in eq. (4) have been determined by a fit subtracting the electronic noise for each beam energy. The sampling fluctuations are then given by

$$S = \sqrt{A_s^2 - A_{tot}^2},$$

where $A_{tot}$ is the resolution found for the sum of the $x$- and $y$-strips, whereas $A_s$ is the average resolution of the $x$- and $y$-strips only. The sampling fluctuations obtained by this method agree within their errors with the results derived from the distribution of the energy difference of the $x$- and $y$-strips (table 6).

*4.1.3. Space resolution for incident pions*

The impact position of pions can be reconstructed with calorimeters of transverse segmentation by a simple center of gravity method as already described in refs. [6,7]. The coordinates are defined by

$$x_{CG} = \frac{\Sigma x_i E_i}{\Sigma E_i}, \qquad (5)$$

where $x_i$ is the coordinate of the centre of tower $i$ and $E_i$ the reconstructed energy with $\pi^0$ weighting in tower $i$.

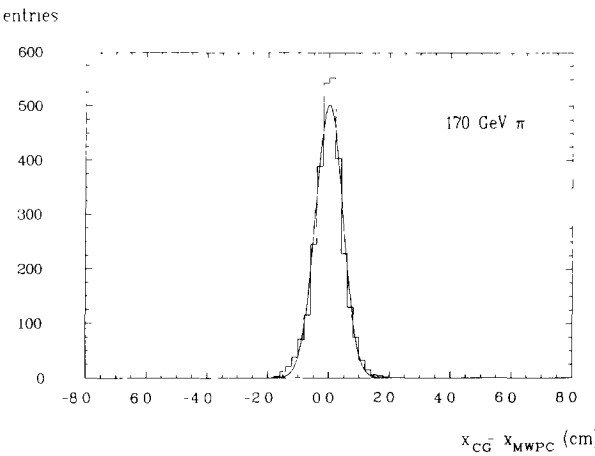


Fig. 7. Distribution of the difference of the impact position reconstructed with the center of gravity and the impact position measured with MWPC at $E_{beam} = 170$ GeV.

If $x_{MWPC}$ is the impact coordinate measured with the multiwire proportional chamber (MWPC, see ref. [1]) the relative impact position distribution $x_r = x_{CG} - x_{MWPC}$ is considered to be a measure of the position resolution $\sigma_p$.

Fig. 7 shows the distribution of the relative impact position $x_r$ for a beam energy of 170 GeV. The position resolution as function of the beam energy is given by the rms of these $x_r$ distributions and is shown in fig. 8. These results are obtained averaging over a range of impact positions of 1.5 cm (corresponding to the hole veto counter [1]). The curve in fig. 8 is a fit by the ansatz

$$\sigma_p = \sqrt{\frac{\sigma_0^2}{E} + c^2} \qquad (6)$$

yielding the results given in table 7. No corrections for

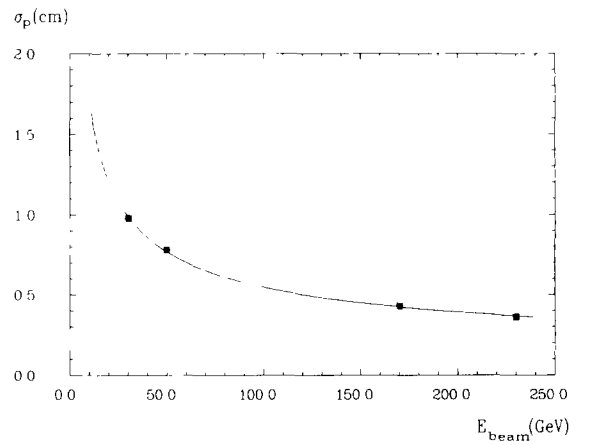


Fig. 8. Space resolution for fully contained events in the LAr calorimeter as function of the beam energy. The curve corresponds to the fit parameters given in table 7.

Table 7
Space resolution obtained by a fit of eq. (6) for various cuts.

| Selection criteria | $\sigma_{0x}$ (cm $\sqrt{\text{GeV}}$) | $c_x$ (cm) |
|---|---|---|
| $E_{TC} \approx 0$ GeV | $5.91 \pm 0.06$ | $0.12 \pm 0.04$ |
| $E_{TC} \approx 0$ GeV, $E_{EC} < 0.05\, E_{beam}$ | $6.89 \pm 0.20$ | $0.29 \pm 0.04$ |
| Without cut | $5.88 \pm 0.06$ | $0.25 \pm 0.02$ |

the bias introduced by the center of gravity method (compare ref. [7]) have been applied. A dependence of $\sigma_p$ on the real impact position has not been observed over the available range of about 3 cm. The observed variation of $\langle x_r \rangle$ over this range is below 0.5 cm. If events are selected which are fully contained in the hadronic calorimeter, which has larger transverse tower sizes, $\sigma_0$ is increased (table 7). Allowing for leakage of the shower energy into the TC leads to an increase of the constant term by nearly a factor of two, whereas the term $\sigma_0$ is essentially unchanged.

Optimizing the rms of the $x_r$ distributions by the introduction of a different weight for the energies in the HC relative to the EC in eq. (5) leads to a reduction of about 15% of $\sigma_0$ for fully contained events in the LAr calorimeter, while $c$ stays the same. Minimal $\sigma_p$ are achieved if this weight factor is about 0.2. However, the number of events outside $3\sigma$ of fitted Gauss distributions increases from about 2% to 3%.

Results on the space resolution of incident electrons in the energy range of 1–5 GeV for the same lead stack have been presented in ref. [8].

### *4.2. Combined results of the liquid argon and tail catcher calorimeters*

The performance of the combined system of the LAr calorimeter with the TC was studied with both calorimeter calibrated as described in section 3.

Fig. 9 shows, for various incident pion energies, $E_{beam}$, the fraction of events with an energy deposit in the tail catcher, $E_{TC}$, larger than a given threshold, $E_{TC}^{th}$, as a function of this threshold. For example, a fraction of $\sim 0.5\%$ of the events deposit more than 50% of the beam energy of 170 GeV in the TC. The energy leaking out of the LAr calorimeter leads to significant tails in the distribution of the energy measured with the LAr calorimeter alone, $E_{LAr}$. This is demonstrated in fig. 10 where $E_{TC}$ is plotted versus $E_{LAr}$ together with a line representing $E_{LAr} + E_{TC} = E_{beam} = 170$ GeV and the projected distributions. A large tail at the low energy side is visible in the spectrum of $E_{LAr}$ in contrast to the events fully contained in the LAr calorimeter.

Since the LAr and the tail catcher calorimeters are separated by an inactive region of $\sim 1.4\lambda$ depth, the

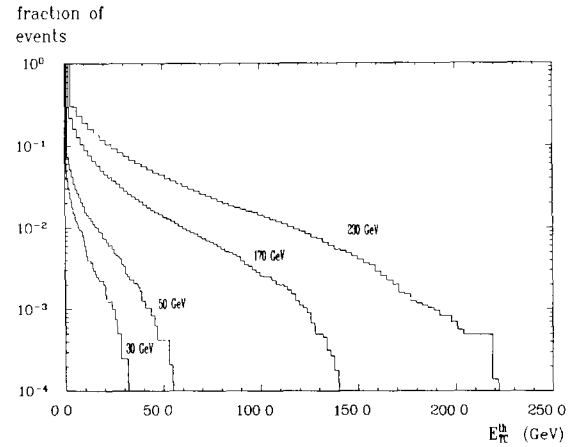


Fig. 9. Ratio of events with a tail catcher energy greater than a given threshold $E_{TC}^{th}$ plotted versus $E_{TC}^{th}$.

correlation between the two calorimeters is off the line representing the beam energy, especially for high energy deposits in the TC. As a consequence, the spectrum of the total energy, $E_{tot} = E_{LAr} + E_{TC}$ still shows a large tail at the low energy side (see fig. 11a).

To achieve a more Gaussian distribution, a correction for the energy loss in the dead region has to be applied. As indicators for large energy losses in the dead region, the last active layer of the LAr calorimeter and several sections of the TC have been investigated. Figs. 12a and 12b, for example, show the energy in the last section of the LAr calorimeter and the number of

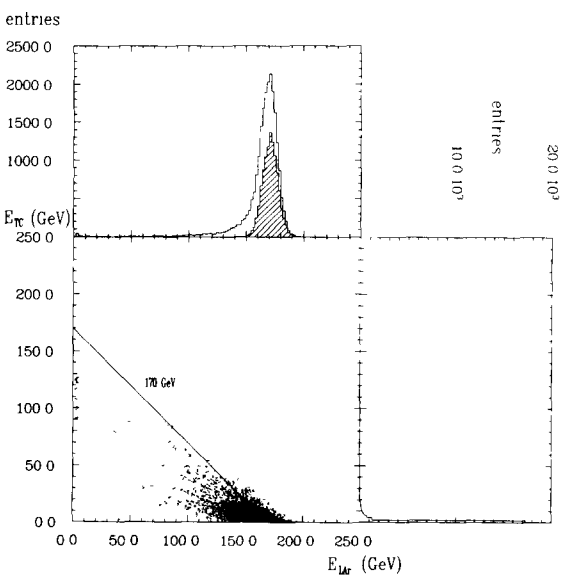


Fig. 10. Tail catcher energy $E_{TC}$ versus LAr energy $E_{LAr}$, together with projections. For comparison, the distribution for the events fully contained in the LAr calorimeter is also given (shaded histogram). See text for details.

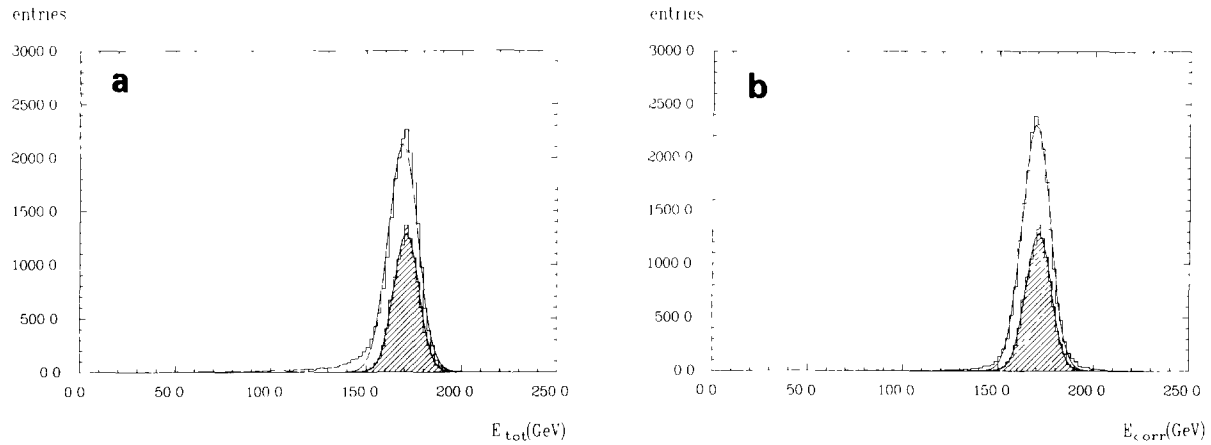


Fig. 11. (a) Total energy $E_{tot}$ in both calorimeters. For comparison, the distribution for the events fully contained in the LAr calorimeter is also given (shaded histogram). (b) Total energy (after correction) $E_{corr}$.

parallel strips fired in the TC plotted versus the total energy. (For these plots, events with hits in the last two layers of the TC have been rejected in order not to mix up the effects of energy still leaking out of the TC with energy loss in the inactive material between the two calorimeters.) Clear correlations are visible. To correct for these correlations, the following ansatz was used:

$$E_{corr} = \alpha E_{tot} + \sum_i \beta_i X_i, \tag{7}$$

where $E_{corr}$ is the corrected energy, $E_{tot}$ is the total energy, $E_{LAr} + E_{TC}$, $\alpha$, $\beta_i$ are correction parameters, and $X_i$ is the information from longitudinal section $i$ (energy or number of strips).

The $\alpha$, $\beta_i$ have been determined by a minimization of

$$\frac{1}{N_{event}} \sum_{j=1}^{N_{event}} \left( E^j_{corr} - E_{beam} \right)^2,$$

the rms resolution of the corrected energy. Using the different sections in both calorimeters, a variety of correction procedures have been investigated [4]. They are listed table 8. The results can be summarized as follows:

(1) A considerable improvement of the energy resolution is only obtained, if for the corrections both the last and the first active section of the LAr calorimeter and the TC respectively are used.

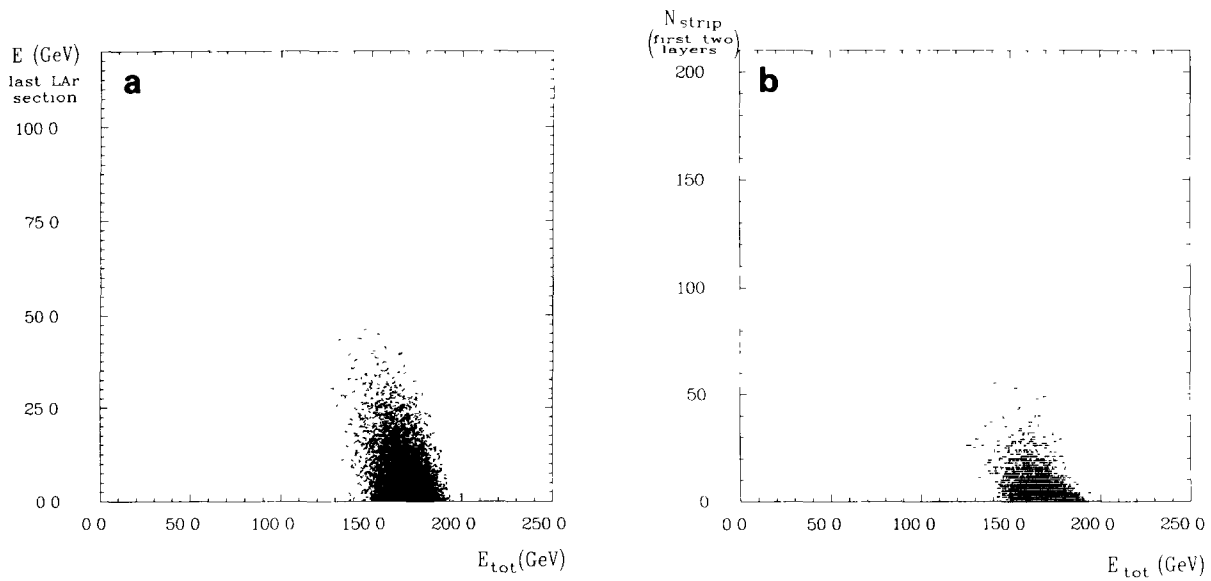


Fig. 12. (a) Energy in the last section of the LAr calorimeter versus the total energy. (b) Number of parallel strips in the first two layers of the tail catcher calorimeter versus the total energy.

Table 8
Calorimeter sections used for the correction of the energy loss in the inactive material between the two calorimeters.

| Case | No. of sections used | LAr calorimeter | Tail catcher calorimeter |
|---|---|---|---|
| 1 | 1 | last section | – |
| 2 | 1 | – | presampler pads |
| 3 | 1 | – | pres. pads plus 1st tower |
| 4 | 1 | – | pres. pads plus all towers |
| 5 | 1 | – | presampler parallel strips |
| 6 | 1 | – | all parallel strips |
| 7–11 | 2 | last section | same as 2–6 |
| 12 | 3 | last section | presampler parallel strips and all pads |
| 13 | 3 | last section | 1st and 2nd tower |
| 14 | 2 | last section, 2nd order | presampler parallel strips |
| 15 | 2 | last section, | presampler parallel strips 2nd order |

(ii) The choice of the TC section is arbitrary. Within the errors, the results agree for the five TC sections which were investigated.

(iii) Taking into account more than one section of the TC does not further improve the results.

Table 9
Correction parameters.

| $E_{beam}$ (GeV) | $\alpha$ | $\beta_1$ | $\beta_2$ |
|---|---|---|---|
| 30 | 0.990 | 0.333 | 0.194 |
| 50 | 0.988 | 0.374 | 0.203 |
| 170 | 0.986 | 0.357 | 0.416 |
| 230 | 0.994 | 0.332 | 0.212 |
| Used parameters | 1.000 | 0.350 | 0.250 |

(iv) The same is true if higher order polynomials in $X$ in eq. (7) are used.

Therefore a correction using the last section of the LAr calorimeter and the number of parallel strips in the first two layers of the TC is applied to obtain the results given below. The parameters $\alpha$, $\beta_i$ for the different beam energies are listed in table 9. Since the results do not critically depend on the absolute value of the correction parameters, the same parameters can be used for all beam energies (table 9).

Fig. 11b shows the energy spectrum after this correction for all events at 170 GeV. Further details are given in table 10, which contains the rms ($\sigma_{rms}$), the resolution ($\sigma_{Gauss}$), mean value ($\langle E \rangle$) and the $\chi^2$ per degree of freedom ($\chi^2$/dof) obtained from a Gaussian fit within $\pm 3\sigma_{rms}$ and the fraction of events outside of $\pm 3\sigma_{Gauss}$ for several cases.

The corrections result in an improved energy resolution. The tails in the energy distributions are considerably reduced. They are, however, still three times larger than for the events fully contained in the LAr calorimeter. Compared to the uncorrected energy distribution, or even the distribution without using the TC, the quality of the Gaussian fits is improved. The correlations visible in figs. 12a and b are also strongly reduced by these corrections (figs. 13a and 13b).

The energy resolutions obtained by Gaussian fits are shown in fig. 14. A parametrization according to eq. (4) results in:

$$A = (0.424 \pm 0.008) \quad \sqrt{\text{GeV}},$$

$$C = (0.029 \pm 0.001),$$

with $B = 1.2$ GeV for the noise contribution in the LAr calorimeter. The results show that the constant term $C$ is larger than in the case of showers fully contained in the LAr calorimeter (section 4.1.1). The fraction of events outside $\pm 3\sigma_E$ is also increased but still below 2.5% at the highest available energies of 170 and 230 GeV.

Table 10
Results for 170 GeV obtained with and without tail catcher and with and without correction to the energy loss in the inactive material.

| | TC empty | All events without TC | With TC uncorrected | With TC corrected |
|---|---|---|---|---|
| $\frac{\sigma_{rms}}{\langle E \rangle}\sqrt{E}$ (% $\sqrt{\text{GeV}}$) | 56.9 | 166.3 | 101.2 | 73.7 |
| $\frac{\sigma_{Gauss}}{\langle E \rangle}\sqrt{E}$ (% $\sqrt{\text{GeV}}$) | 50.3 ± 0.5 | 63.1 ± 0.3 | 60.5 ± 0.3 | 56.8 ± 0.3 |
| $\langle E \rangle$ (GeV) | 170.95 ± 0.07 | 168.58 ± 0.06 | 169.16 ± 0.06 | 169.51 ± 0.05 |
| $\xi^2$/dof | 1.7 | 42.9 | 28.4 | 2.8 |
| Outside of $\pm 3\sigma_{Gauss}$ (%) | 0.92 | 8.4 | 5.1 | 2.5 |

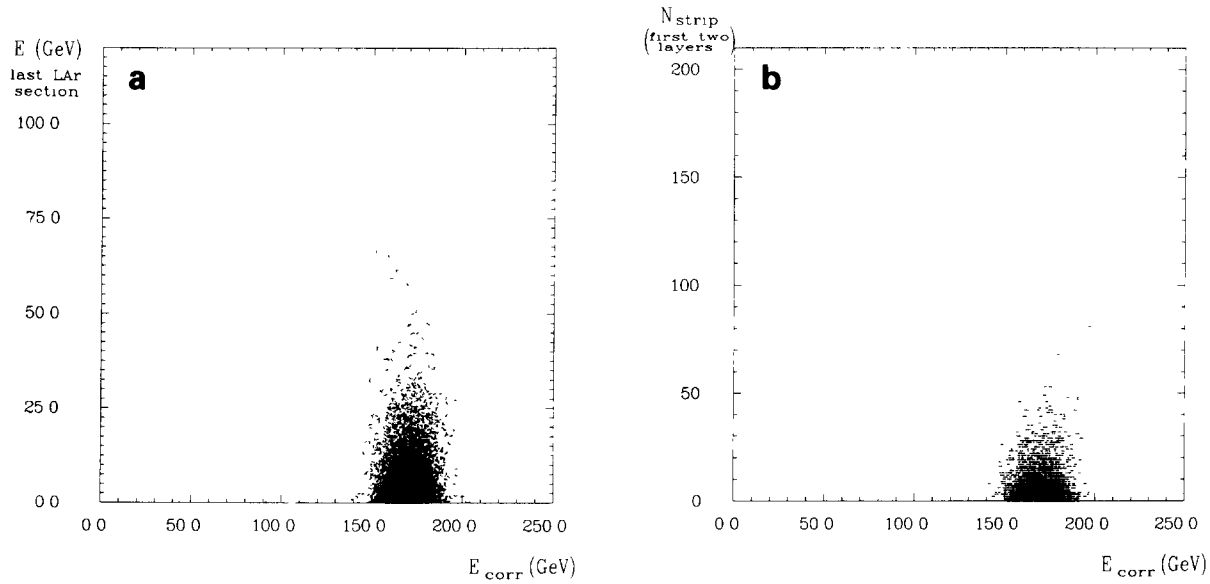


Fig. 13. (a) Energy in the last section of the LAr calorimeter versus the total energy after correction. (b) Number of parallel strips in the first two layers of the tail catcher calorimeter versus the total energy after correction

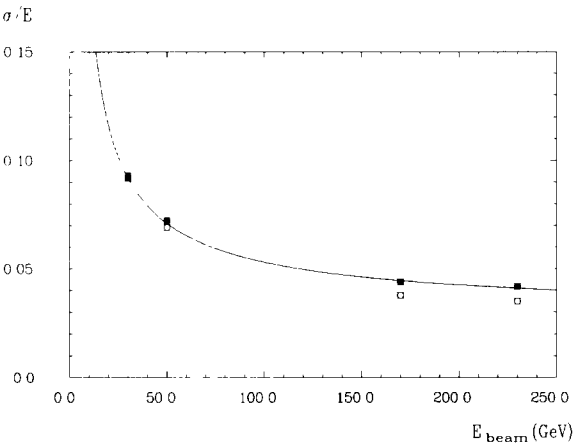


Fig. 14. Energy resolution of the combined system of LAr calorimeter and TC (full symbols) versus beam energy. The curve corresponds to the parametrization given by eq. (4) with $A = 0.424\ \sqrt{\text{GeV}}$, $B = 1\,2$ GeV and $C = 0.029$. The open circles represent the events fully contained in the LAr calorimeter.

## 5. Conclusions

The performance of a lead–copper LAr calorimeter (6.1λ) together with an iron streamer tube tail catcher (4.5λ) has been tested with pions in the energy range of 30–230 GeV. The energy resolution is considerably improved by corrections for $\pi^0$ fluctuations on an event to event basis. The energy dependence of the resolution can be described by

$$(\sigma/E)^2 \approx (0.45/\sqrt{E})^2 + (1.2/E)^2 + C^2$$

with $C = 0.016$ for showers fully contained in the LAr calorimeter and $C = 0.029$ without this requirement. For showers with significant energy leakage into the tail catcher corrections are necessary for the energy loss in the dead material (1.4λ) between the two calorimeters. With these corrections the fraction of events outside $\pm 3\sigma$ of the measured energy distribution is below 2.5% for pion energies up to 230 GeV.

The energy resolution of the copper section of the liquid argon calorimeter (5 mm Cu plates) has a sampling contribution of approximately $0.24/\sqrt{E}$.

The space resolution for incident pions is found to be 6 cm$/\sqrt{E}$.

## Acknowledgements

We would like to thank all the technical collaborators for their help and their contributions to the test of the calorimeters. The support of the CERN staff operating the SPS, the H6 beam line and computer facilities is gratefully acknowledged.

## References

[1] W. Braunschweig et al., Nucl. Instr. and Meth. A265 (1988) 419;
DESY 87-098.
[2] W. Braunschweig et al., Nucl. Instr. and Meth. A270 (1988) 334.
[3] J Marks, Dissertation, Universität Hamburg (1988), in preparation.

[4] E. Vogel, Dissertation, RWTH Aachen (1988), in preparation.
[5] CDHS collaboration, Nucl. Instr. and Meth. 180 (1981) 429.
[6] A. Babaev et al., Nucl. Instr. and Meth. 160 (1979) 427.
[7] V.A. Davidov et al., Nucl. Instr. and Meth. 174 (1980) 369.
[8] C. Zeitnitz, Internal Report, DESY F21-01 (1988).
[9] H1 Collaboration, Ch. Berger et al., Technical Proposal for the H1 Detector, DESY 1986 and Technical Progress Report, DESY 1987, both unpublished.